Glare Point Velocimetry and Sizing (GPVS)
Introduction of a new optical 2D measuring technique for bubbly flows

by S. Dehaeck[1,2], J.P.A.J. van Beeck[1]and M.L. Riethmuller [1]

[1] Von Karman Institute for Fluid Dynamics
Waterloose Steenweg 72, B-1640 Sint-Genesius-Rode, Belgium
[2] Dept. of Flow, Heat and Combustion Mechanics
Ghent University
St.-Pietersnieuwstraat 41, B-9000 Gent, Belgium
E-mail: dehaeck@vki.ac.be

ABSTRACT

A novel measuring technique for bubbly flows, named Glare Point Velocimetry and Sizing (GPVS), is presented. It is based on the appearance of regions of higher light intensity coming from reflection and refraction of the incoming laser-light at the surface of the bubble, the so called glare points. With this technique, both the size and the velocity of the bubbles (or droplets) can be measured in a 2D plane. The accuracy of the size determination was shown to be at least equal to that of backlighting and velocity measurements will typically have the accuracy of standard PTV-measurements. All this information is obtained in a 2D plane under a scattering angle of 96° (for air-water) and with a single camera as is shown in Figure 1(a). In addition, this technique is easily extended to yield extra information concerning the bubble, i.e. its refractive index or the non-sphericity of the bubble. This extension also enables us to measure accurately the bubble size under an observation angle of 90°.

Several experiments were performed to validate the technique. To verify the accuracy of the size determination under 96°, a simultaneous comparison with backlighting was performed, which showed that both techniques agree within 1,3%. Under 90°, this comparison resulted in an even smaller error of 1%. The measured relative refractive index differed only 1,3% from the value obtained by Ramuzat [2002]. In addition, the velocity computed with the given technique was in agreement with the correlations given in Clift et al. [1978].

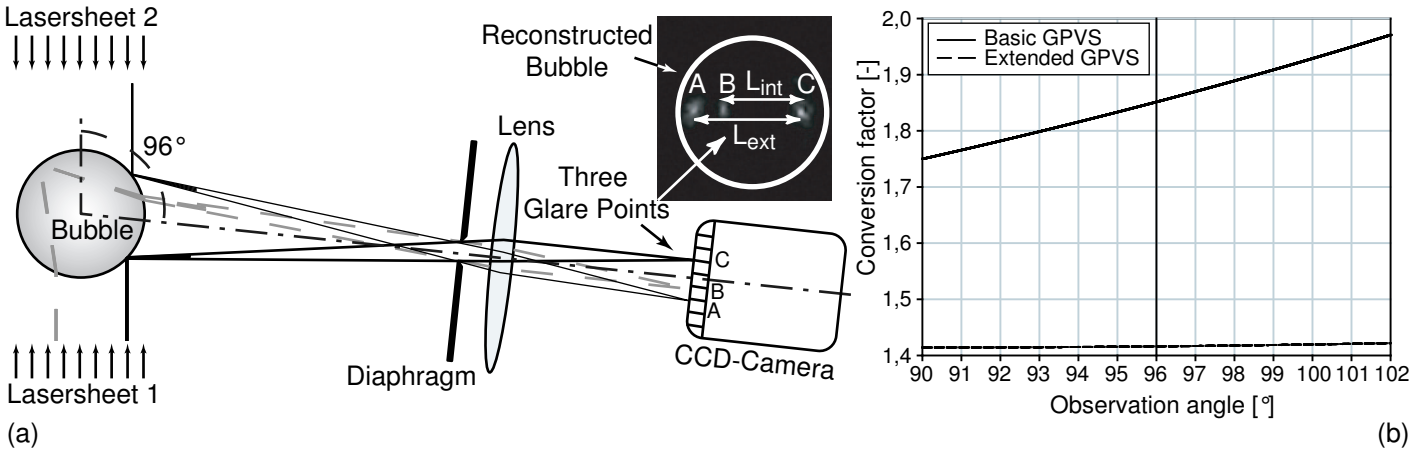

Figure 1: (a) Principle of extended GPVS (b) Conversion factor versus observation angle

1 Introduction

One of the reasons why bubbly flows are very complex is that the forces exerted on the bubbles are mainly coming from the surrounding fluid and not from the inertia of the bubble itself. Therefore, a thorough understanding of the interaction between the bubbles and the fluid is needed for numerical predictions. To this end a 2D experimental technique is necessary, which is able to give accurate information concerning both speed and diameter of the bubbles *as well as* the speed of the surrounding fluid.

There exist a number of techniques today, which give parts of the required information. Backlighting is one of these. It is a well known technique that simply records the shadow images of diffusively illuminated bubbles. However, this technique is not truly 2D since there is no possibility to distinguish between bubbles close or far away from the camera. This lack of localisation in the third dimension results in an impossibility to determine the void fraction. Another, more recent technique is ILIDS (Koenig et al. [1986], Glover et al. [1995]). This technique was originally applied to sprays but has been adapted to bubbly flows by Niwa et al. [2000]. It is based on the interference pattern observed when reflection and refraction spots on the bubble surface are seen out of focus. This technique is able to give very accurate size information while maintaining a large field of view. However, since the interference pattern is 100 to 1000 times bigger than the actual bubble, only low void fractions can be measured. This has been partially improved by Akasaka et al. [2002] through optical compression of the images. Nevertheless, even with this improvement, velocity measurements remain poor and in some cases (Dantec Dynamics [2003] and Damaschke et al. [2002]) a second camera is used to observe the glare points in focus to yield accurate velocity information. This renders the setup more cumbersome and prone to the introduction of new errors. The extension of this technique to measure the velocity of the surrounding fluid will most probably require the use of yet another camera.

The technique that is introduced in this paper is based on the same principles as ILIDS, namely the appearance of glare points at the surface of a bubble placed in a coherent light source. Where these bright spots were observed *out* of focus in ILIDS to observe their interference pattern, they will be observed *in* focus in our technique. This will result in the ability to measure in higher void fractions *and* to determine the velocity more accurately than in ILIDS with a simpler setup. The basic principle for this technique was already mentioned by Hess [1998] for sprays, together with ILIDS. At the time however, the limited resolution of the CCD-cameras rendered the ILIDS-experiments more accurate, thus placing the in-focus technique in the background. In the present study, this technique was adapted to bubbly flows and extended in order to reject misreadings and eliminate the influence of camera misalignment.

2 Theoretical Background

2.1 Basic GPVS

The simple fact that light is reflected and refracted by a bubble has been known for ages, however, a rigorous theoretical basis for this phenomenon was only given by van de Hulst and Wang [1991]. With this theory one is able to predict the expected intensity profile measured by a camera. However, since the measurement principle is not based on the detailed intensity information but only on the location of the glare points, raytracing calculations can be used as was done by van de Hulst and Wang [1991].

In order to determine the best observation angle for our technique, raytracing calculations were performed for linearly polarised laser light with the polarization plane in the observation plane (i.e. parallel). This result is shown in Figure 2, where N stands for the amount of interactions of the light ray and the bubble surface. This figure shows that for an observation angle of 96° the externally reflected light (N=1) and the internally reflected light (N=3) are equally intense. At the same time, the higher order interactions have an intensity that is about two orders of magnitude lower. This is exactly what we need to distinguish both peaks from the background noise and, in addition, this angle is close to 90°, which reduces the projection error on the velocity determination.

A sketch was made of the setup at this observation angle in Figure 3(a). Here we see, how both glare points lie more than one bubble radius apart from each other. It is interesting to note that the width of both peaks is different and hence most probably does not allow an extraction of the bubble size (as has been done by Zimmer [2001]). The basic principle of GPVS now is to multiply the distance between these two sharp intensity peaks with a calculated conversion factor α to derive the bubble diameter. This conversion factor was derived from raytracing with the following formulas:

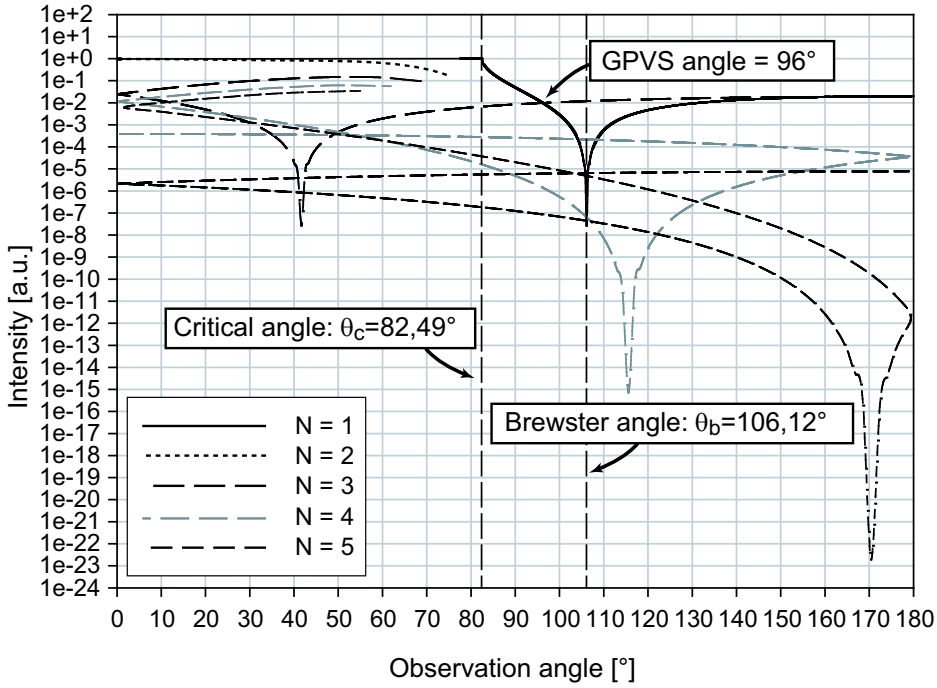

Figure 2: Light intensity versus observation angle for air bubbles in water (n=1,33)

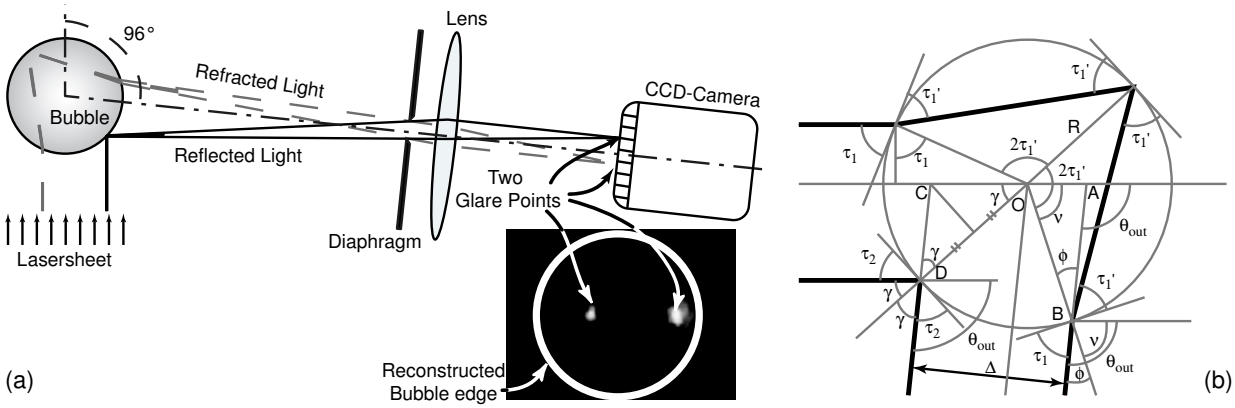

Figure 3: (a) Schematic setup of a basic GPVS measurement (b) Illustration of raytracing variables

$$
\begin{aligned}
\theta_{out} &= 2\tau_1 - 2\left(N-1\right)\tau_1' \\
n_{particle}\cos\left(\tau_1'\right) &= n_{medium}\cos\left(\tau_1\right) \\
\nu &= 4\tau_1' - \tau_1 - \frac{\pi}{2} \\
\gamma &= \frac{\pi}{2} - \frac{|\theta_{out}|}{2} \\
|AC| &= \frac{R\sin\left(|\theta_{out}| - \nu\right)}{\sin\left(|\theta_{out}|\right)} + \frac{R}{2\cos\left(\gamma\right)} \\
\Delta &= |AC|\sin\left(|\theta_{out}|\right) \\
\alpha &= \frac{2R}{\Delta} = \left[\frac{\sin\left(|\theta_{\mathrm{out}}|\right)}{4}\left(\frac{2\sin\left(|\theta_{\mathrm{out}}| - \nu\right)}{\sin\left(|\theta_{\mathrm{out}}|\right)} + \frac{1}{\sin\left(\frac{|\theta_{\mathrm{out}}|}{2}\right)}\right)\right]^{-1}
\end{aligned}
$$

The used symbols are depicted in Figure 3(b). If we impose the observation angle θ_{out}, a value for τ_1 and τ_1' can be obtained numerically. Inserting this value in the angles ν and γ allows us to calculate the distances $|AC|$ and Δ in function of the radius of the bubble. From this, we can extract the multiplication factor α to convert the measured distance Δ into the diameter of the bubble. This derivation assumes the bubble is spherical and, as we can see in the formulas, α depends on the observation angle and the relative refractive index but not on the absolute diameter of the bubble. Its dependence on the observation angle is shown in Figure 1(b). Applying this formula to an air bubble in water ($n_{rel} = \frac{1}{1{,}33}$) results in $\alpha = 1,8517$ at 96°. A misalignment of 1° leads to a maximum error of 1,0% in α and therefore a careful adjustment of the recording camera is recommended.

2.2 Extended GPVS

2.2.1 Higher accuracy

As mentioned, the basic GPVS-technique also depends on the refractive index of the medium. This means that this technique cannot be easily applied to flows with a strong thermal gradient (in the bubble or droplet) or for opaque particles. Therefore, the basic technique was extended to be able to cope with such flows. Its principle is shown in Figure 1(a). For this, a second laser-sheet is used with the opposite sense as the first, which creates additional glare points under a supplementary angle of 84°. From Figure 2 we obtain that only 1 very bright external reflection glare point will be created by the second laser, with a second, much less intense refraction peak. The trick now is to make sure that this extra reflection peak has the same intensity as the two basic glare points coming from the first laser-sheet. Like this, two distances can be measured: the distance between the two externally reflected glare points (denoted by L_{ext} in Figure 1(a)) and the traditional distance (L_{int}). Extended GPVS now uses L_{ext} to determine the bubble size. The conversion factor in this case can be obtained theoretically in a similar way than for basic GPVS and leads to the following formula:

$$
\alpha = \left[\frac{\sin\left(|\theta_{\mathrm{out}}|\right)}{4}\left(\frac{1}{\cos\left(\frac{|\theta_{\mathrm{out}}|}{2}\right)} + \frac{1}{\sin\left(\frac{|\theta_{\mathrm{out}}|}{2}\right)}\right)\right]^{-1}
$$

This factor only depends on the observation angle (Figure 1(b)) and equals 1,4162 at 96°. Using this distance to calculate the bubble diameter enables us to achieve a higher accuracy because it is:

Virtually insensitive to misalignment: The dependency on the observation angle is even smaller in this case (a relative error in α of 0,05% versus 1,00% for basic GPVS for a misalignment of 1°)

Insensitive to the refractive index: No refracted light is used (⇒ possibility to measure opaque particles!)

Less sensitive to non-sphericity: For an aspect ratio of 0,9 the maximum relative error in α equals in this case 11,4% instead of 16,8% for basic GPVS

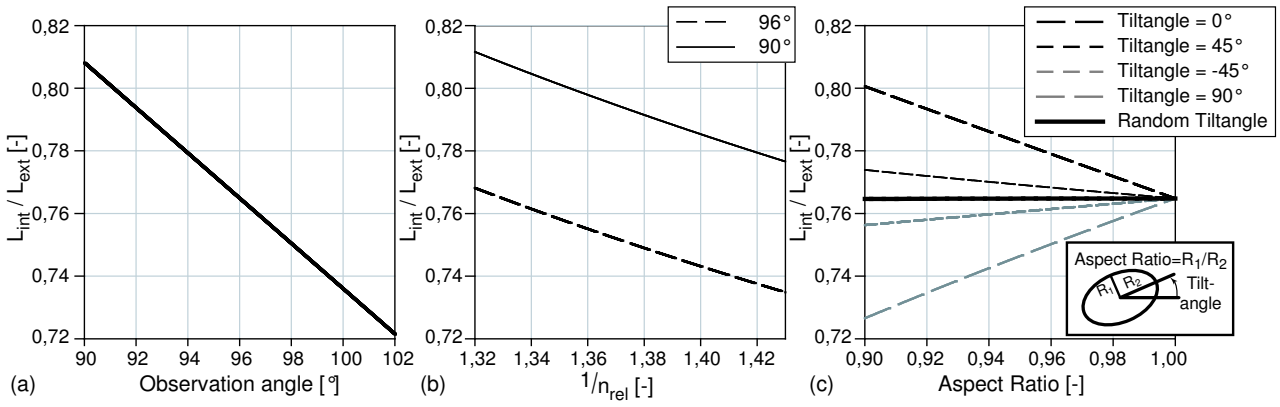

Figure 4: Dependencies of the relative position on (a) observation angle for spherical particles with $\frac{1}{n_{rel}} = 1,33$, (b) relative refractive index for spherical particles and different angles and (c) non-sphericity (aspect-ratio and tilt angle) at 96° and $\frac{1}{n_{rel}} = 1,33$

2.2.2 Extra information

However, the relative location of the third glare point gives us additional information concerning the bubble. In fact, we found that this relative position depends mainly on the *observation angle*, the *relative refractive index* and on the *non-sphericity* of the bubble (aspect ratio and tilt angle) in the observation plane. This relative position is given as the division of both distances versus the mentioned parameters in Figure 4 . We notice that the strongest influence comes from the observation angle, followed by the non-sphericity and the refractive index. This information can be used to one of the following goals:

verification of the alignment: We could first take the average distance ratio of a large number of bubbles. The influence of including non-spherical bubbles is diminished by the superposition of many different tilt angles (this principle is also used in global rainbow thermometry (van Beeck et al. [1999])). The proof for this assumption is also shown in Figure 4(c), where the solid curve represents the average distance ratio taken over all possible tiltangles. This shows that the non-sphericity influence cancels out if all tiltangles are randomly encountered. Inserting this averaged ratio in Figure 4(a) gives us a better estimate of the real observation angle. This can be used to better align the system or obtain a better conversion factor accordingly.

extract average temperature: If we assume that the alignment of the camera is perfect, we could extract from the averaged ratio an estimation of the relative refractive index from Figure 4(b) and hence of the average temperature of the considered bubbles.

extract per bubble temperature or non-sphericity: After using the averaged distance ratio in one of the above mentioned ways, the per bubble ratio could be used to give its temperature (if spherical) or its aspect ratio if the tilt angle is assumed.

Rejection of misreadings: The per bubble ratio could also be used to reject bubbles that are significantly non-spherical since in this case the error on the calculated spherical equivalent diameter becomes too large. Also misreadings coming from spurious reflections on the surface of the bubble, can be detected in this way. Such reflections come from laser light that is already deflected by other bubbles. In general, such reflections will have a markedly lower intensity and their appearance will almost certainly result in a different glare point pattern than expected, allowing them to be detected and dealt with.

2.2.3 Different observation angles

With the use of a second laser-sheet, different angles can be used as well and in particular, an observation angle of 90° is possible. From Figure 2 we obtain that at 90° only the externally reflected light is important. Thus, with two equally intense laser-sheets we would obtain two bright glare points per bubble, independent of the refractive index and of the observation angle (0,007% for 1° misalignment). However, it is very likely that the internally reflected glare points are no longer visible and that we lose the ability to extract extra information.

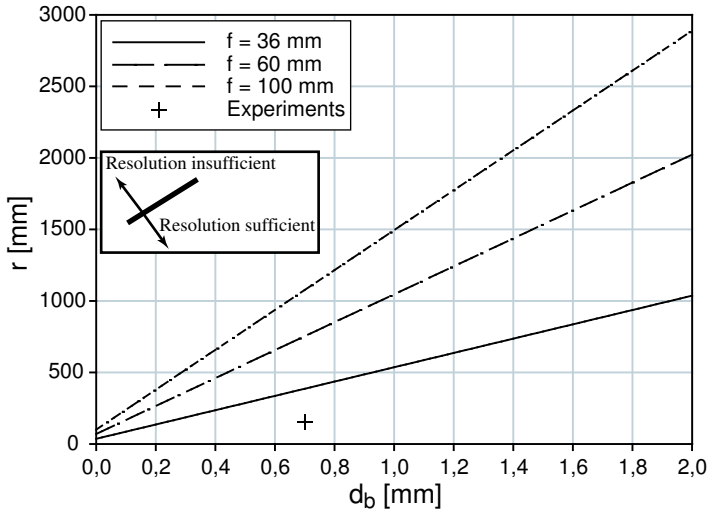

Figure 5: Magnification requirements for basic GPVS

2.3 Experimental setup considerations

One of the main obstacles of applying this technique in real life situations is the necessity to observe both (or all three) the glare points distinctly, which requires a sufficiently large magnification factor. Therefore, a small study of what is already feasible today will be given next (which follows the derivation by Theunissen [2003]).

In the limit of a camera placed on an infinite distance, the width of each glare point is solely determined by the diffraction imposed by the diaphragm. However, both glare points should not be allowed to overlap since their interference pattern will result in the appearance of extra peaks that might render a correct measurement impossible and would surely make the sub-pixel fitting incorrect. Assuming that each glare point corresponds to a peak of approximately three pixels on the CCD-camera (which allows a Gaussian fitting) through a correct setting of the diaphragm, this implies that the location of the two peaks should be a minimum of 4-5 pixels apart. Knowing that the multiplication factor for basic GPVS is approximately 2, this would require that the image of the bubble on the CCD-camera should span roughly 10 pixels. From the thin lens formulas we obtain the following restriction:

$$r \leq f + \frac{f \times d_b}{10 \times w_{pix}}$$

where r is the distance of the camera to the bubble, d_b is the bubble diameter, f is the focal length of the camera and w_{pix} is the width of a pixel in the camera. In the Canon Powershot G3 (which was used in our experiments) this equals 7 μm. With this value we can plot a curve of the maximum separation distance in function of the size of the bubble and this for different focal lengths of the camera. Such a graph is shown in Figure 5 , with the curve $f = 36\,\mathrm{mm}$ corresponding to the camera setting during our experiments. The complete experimental condition is also indicated in this figure by a cross-hair, using the smallest encountered bubbles in our experiments (0,7 mm). Theoretically the camera could have been placed at a distance of 386 mm in our experiments. However, we chose to put our camera as close as possible (r=155 mm), in order to obtain a higher accuracy in the size determination. At this distance, the smallest bubble diameter that could have been measured is 0,2380 mm. Using for instance a lens with a focal distance of 100 mm would allow a separation of 1 m and at a separation of 155 mm the smallest detectable bubbles are only 39 μm! Of course, for extended GPVS this restriction is even more severe since the distance between the closest peaks is roughly one sixth of the bubble diameter. This renders the correctly detectable bubbles to be two to three times larger than what is indicated in the figure. For our separation distance and focal length, this implies a minimum detectable bubble diameter with extended GPVS of 0,7143 mm (0,12 mm for a 100 mm lens).

Next to the smallest detectable bubbles, there is also the question of accuracy. Since the localisation error of the peaks is independent of the separation between peaks, the accuracy of the technique will improve if the bubble corresponds to more pixels (i.e. a higher magnification). This means that there is a trade-off between accuracy and field of view (similar

to backlighting). In our experiments, a single pixel (and more or less the uncertainty) corresponded to $\frac{1}{42}$ of a mm, which resulted in a field of view of 5,4 x 4 cm with our 4 megapixel camera. This is already quite acceptable. Furthermore, the continuing improvement of the CCD-cameras concerning pixel-size and total amount of pixels will only help to enlarge the working domain of GPVS. Its lower limit being determined by the minimum separation distance and the required accuracy whereas its upper limit is determined by the spherical assumption. For bubbles this limit is usually taken at approximately 1 mm. However, at this size the cross-section in a *vertical* plane loses its circularity but GPVS assumes a circular *horizontal* cross-section, which is likely to hold even longer.

3 Experiments

3.1 Goals

To verify the validity of the above numerical and theoretical statements, several experiments were performed. First, the size determination with basic GPVS was verified through simultaneous measurements with backlighting on air bubbles in a water tank. Then, velocity and size measurements were performed and this result was compared to a correlation of the terminal velocity versus the diameter taken from Clift et al. [1978]. To prove the usability of extended GPVS, measurements were performed on an air bubble entrapped in a silicone block. The refractive index of the silicone block was measured with the new technique and the theoretically obtained dependency on the observation angle was experimentally verified. Finally, a simultaneous measurement with backlighting was performed on the silicone block under an observation angle of 90°.

3.2 Experimental setup

As already mentioned, some tests were performed on air bubbles in a water tank, some were performed on a bubble entrapped in a silicone block. The experimental setup with the water tank is shown in Figure 6. For backlighting a normal light bulb with a diffuser plate and a colour filter (which stops red light) was used. With the use of a simple red continuous Helium-Neon laser, this enables us to perform backlighting and GPVS at the same time, and separate both techniques by the use of a simple colour CCD-camera, in our case the Canon Powershot G3. The observation angle was measured with an angular positioning device with an accuracy of 1°. The 90° reference was obtained by replacing the camera with a laser and aligning the reflected beam with the original one at a large distance. Furthermore, we notice that the observation angle used in these experiments was not 96°, as was mentioned several times before, but 98°. This is simply because the parallel lines get deflected while exiting the water tank.

For the extended GPVS experiments, the water tank was replaced by the silicone block. The second laser-sheet that is needed for extended GPVS, was simply the reflection of the original laser-sheet while leaving the silicone block. This creates almost perfectly the desired glare point intensity. In the water tank, the reflection of the primary laser-sheet on the Plexiglas wall created the third glare point as well. This was not desired however, since it partly merged with the internal reflection spot and therefore a metal plate was inserted at the right of the water tank to reflect the primary laser-sheet in another direction.

3.3 Results

3.3.1 Size Calibration basic GPVS

A typical figure is given in Figure 7. By extracting the red channel for the GPVS measurement and using the green channel to perform backlighting, a verification of the technique can be performed under realistic conditions. An important advantage of such an approach is the fact that this comparison does not include any error made in the determination of the magnification factor of the camera, since the bubble size is obtained in pixels. These red and green figures were then processed in the following way:

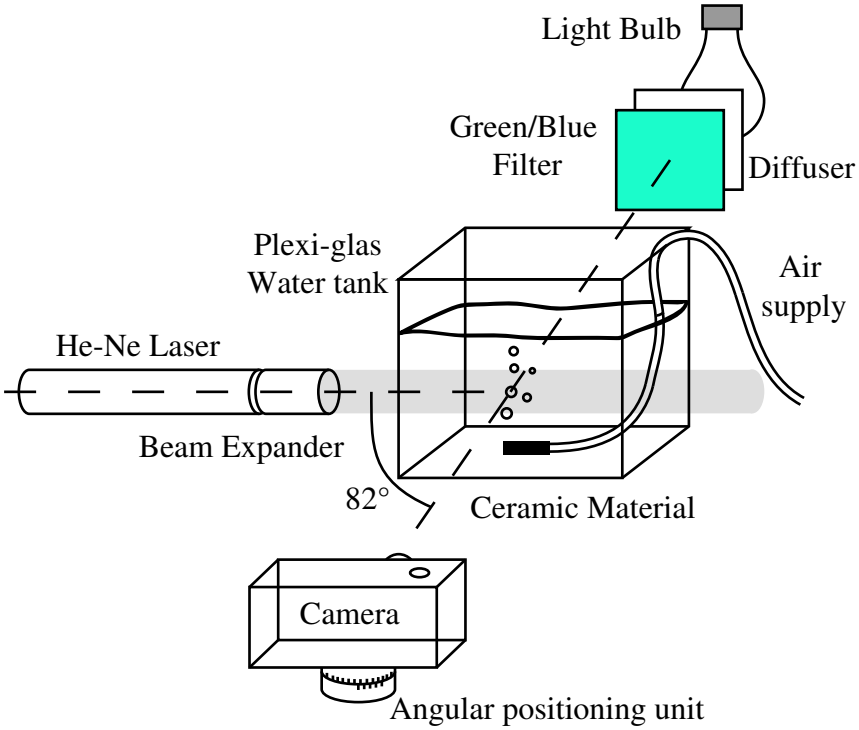

Figure 6: Experimental setup for the water experiments

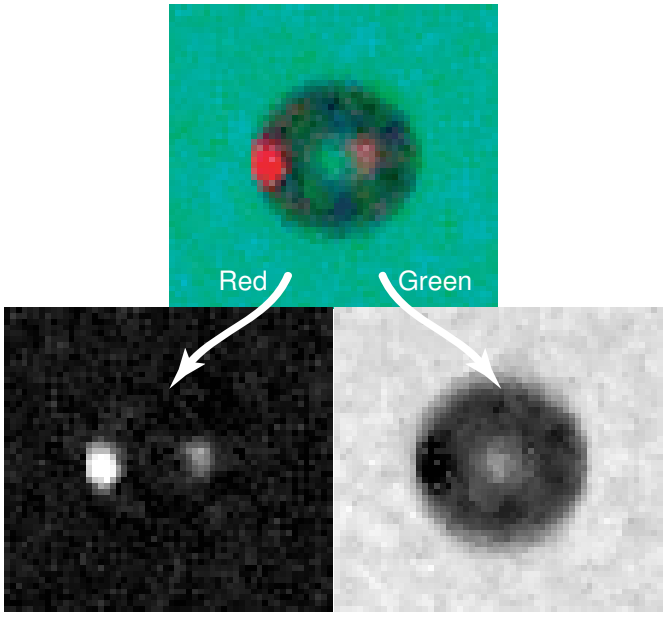

Figure 7: Typical colour picture obtained from basic GPVS (red) with simultaneous (green) backlighting ($f_\sharp = 3$, $M = 0,3011$ and $\text{shutter speed} = \frac{1}{1250}$s)

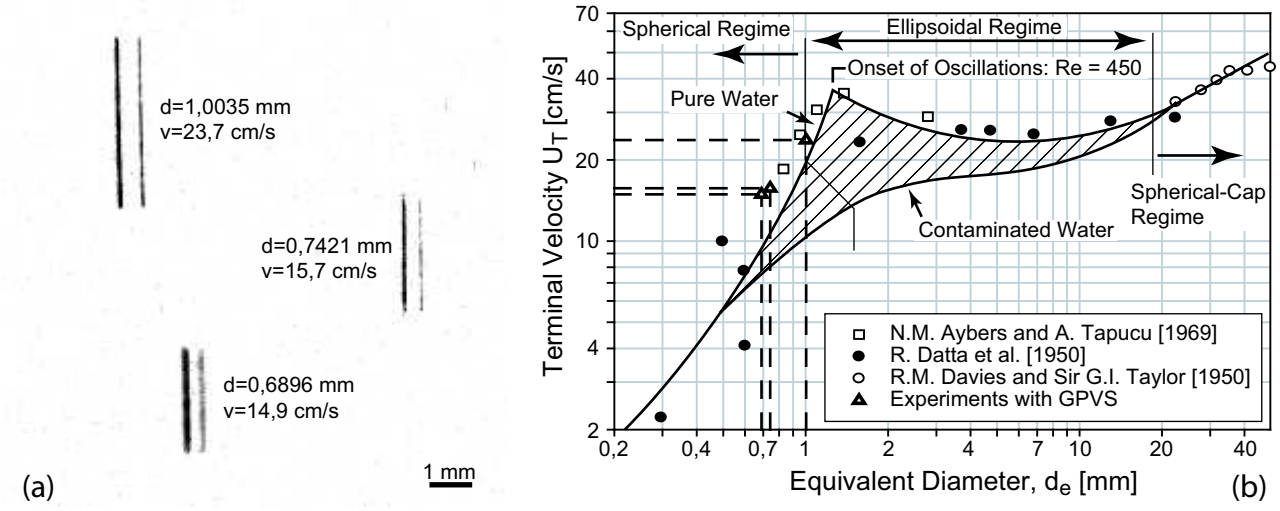

Figure 8: (a) Streak velocimetry performed with basic GPVS ($f_\sharp = 5$, $M = 0,3011$ and $\text{shutter speed} = \frac{1}{60}$s) (b) Comparison of the obtained velocities with a reproduction of the correlation from Clift et al. [1978] p. 172 along with the experiments of Aybers and Tapucu [1969], Davies and Taylor [1950], Datta et al. [1950]. The current experiments with GPVS are indicated with open triangles and droplines

GPVS: The peaks were Gaussian fitted to obtain a sub-pixel accuracy of their location and then their separation was multiplied by the obtained conversion factor and with a supplementary factor (=0,998) coming from the deflection of the parallel beams at the Plexiglas wall.

Backlighting: First the Sobel filter was applied to the picture in order to correctly detect the edges. The edge was assumed to be at the location of the maximum gradient and was Gaussian fitted accordingly, which is a fair approximation of the true edge. A more exact localisation is only possible through a rigorous theoretical derivation with the generalised Lorenz-Mie theory, which was not performed here. In addition, the same supplementary factor as above coming from the deflection at the Plexiglas wall had to be applied on this diameter.

For the displayed bubble this leads to a difference in the calculated radius of 1,3% (0,1 on a total of 7,6 pixels). Considering the approximation that is used to determine the bubble edge location in backlighting, an error of 0,2 pixel in the diameter is certainly negligible. Note also, that this setup allows us to measure the bubble in 3 dimensions and that an accurate volume measurement could have been performed.

3.3.2 Velocity calibration basic GPVS

For measuring the velocity with GPVS there are basically two different approaches: PIV-like and streak velocimetry. Although streak velocimetry is certainly inferior to the PIV-approach, it was still used here in view of the simple setup used for our experiments. Using a shutter speed of 1/60 s and no backlighting, the two peaks transformed into two parallel lines as can be seen in Figure 8(a). The size determination was performed as explained before on a randomly selected height. This result was then placed in a correlation of the terminal velocity of a free rising bubble versus its diameter from Clift et al. [1978] in Figure 8(b). We notice that our velocities are systematically higher than the proposed correlation, although similar results are also included in this graph coming from other authors. The reason for this 'overshoot' probably comes from the fact that our bubbles move in a bubble train and therefore are expected to obtain higher velocities than a single bubble in stagnant water.

3.3.3 Extended GPVS verification

For a verification of the principles of the extended GPVS technique, we chose to reproduce the curve of Figure 4(a) experimentally and determine the behaviour of the distance ratio versus the observation angle. However, as was already

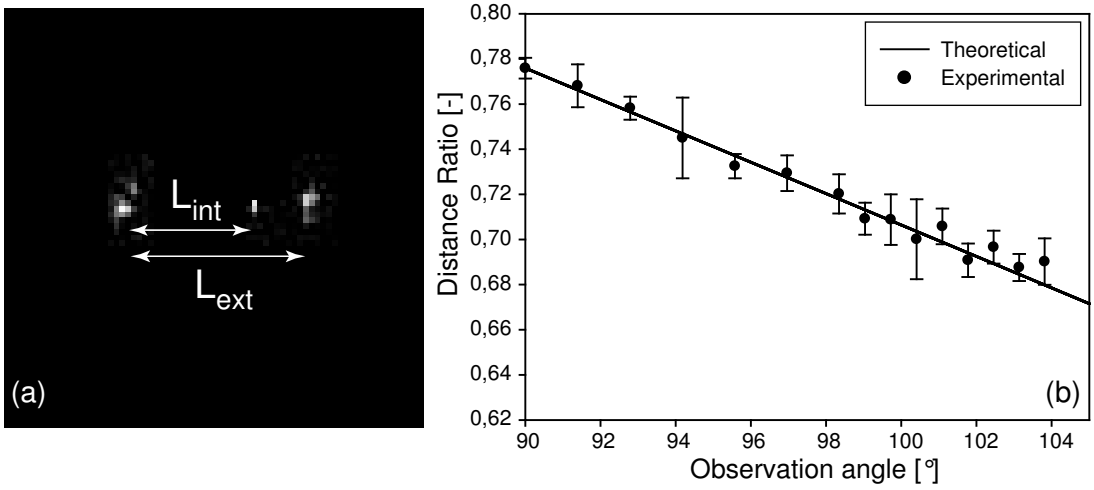

Figure 9: (a) Extended GPVS performed on an entrapped air bubble in silicone with $f_\sharp = 8$, $M = 0,3011$ and $\text{shutter speed} = \frac{1}{400}$s (b) Comparison of experimental and theoretical distance ratio versus observation angle

mentioned in 2.3, the limited magnification of the used camera often resulted in partially overlapping glare points with extended GPVS. Now, in order to have a higher accuracy in the ratio determination and to be able to adjust the observation angle more easily, a larger static spherical bubble (2,23 mm) was created inside a silicone block. A typical extended GPVS picture is shown in Figure 9(a), with the primary laser-light coming from the left.

Before we can compare the experimental dependency on the observation angle with the theory, we first need the refractive index of the silicone. Earlier experiments performed by Ramuzat [2002] with a prism made from the same material yielded a refractive index of $1,414 \pm 0,033$. In order to demonstrate the ability of extended GPVS to measure the relative refractive index, this value will be extracted from the relative position of the internal reflection glare point at an observation angle of 90° (since the laser-light is not deflected while leaving the silicone block at this angle). Thus, we obtained an average ratio of 0,7759 (taken over 5 pictures). From a theoretical plot of the distance ratio versus the refractive index at an observation angle of 90° (shown in Figure 4(b)), we found that the refractive index of the silicone must be 1,4325. This value only differs 1,3% from the value obtained by Ramuzat [2002] and lies well within their stated uncertainty.

Then, several pictures were taken at effective angles of 90° to 110°, thus including the additional deflection of the laser while leaving the silicone block. These distance ratios were then plotted against the theoretical ratio versus the observation angle (before deflection) computed with the previously obtained refractive index of the silicone (by GPVS) in Figure 9(b). The error bars that are shown in this figure are the standard deviations from several pictures and hence do not include any misalignment errors. The experiments agree within 1,5%, with higher errors appearing for larger angles. This is explained by the emergence of extra glare points at this point, which rendered a sub-pixel interpolation impossible, as could be clearly seen in these pictures. We would like to stress that this good agreement was obtained while maintaining a field of view of 5,4 x 4 cm. If a better accuracy is needed, higher magnifications are still possible.

3.3.4 Extended GPVS under 90°

This experiment was also performed on the silicone block and the second laser-sheet was created by enhancing the reflection of the primary laser-sheet at the silicone wall with a mirror. A simultaneous measurement with backlighting was performed as well, in order to test the accuracy of the technique. The green and red channel are shown in Figure 10(a) and (b), where the contrast of the green channel was enhanced for printing purposes. In (c) a horizontal profile of the red channel at the centre of the bubble is shown. Due to the high saturation of the *external* reflection spots, the less intense *internal* reflection spots are still clearly visible and extraction of extra information is still possible. The conversion factor for this case is 1,4142 and no correction due to deflection should be applied. Both techniques agreed again within 1 % (0,24 on a radius of 23,43 pixels). This comparison was not performed on the shown picture though, since the high saturation made a sub-pixel interpolation impossible. Instead, a different picture with almost no saturation was used.

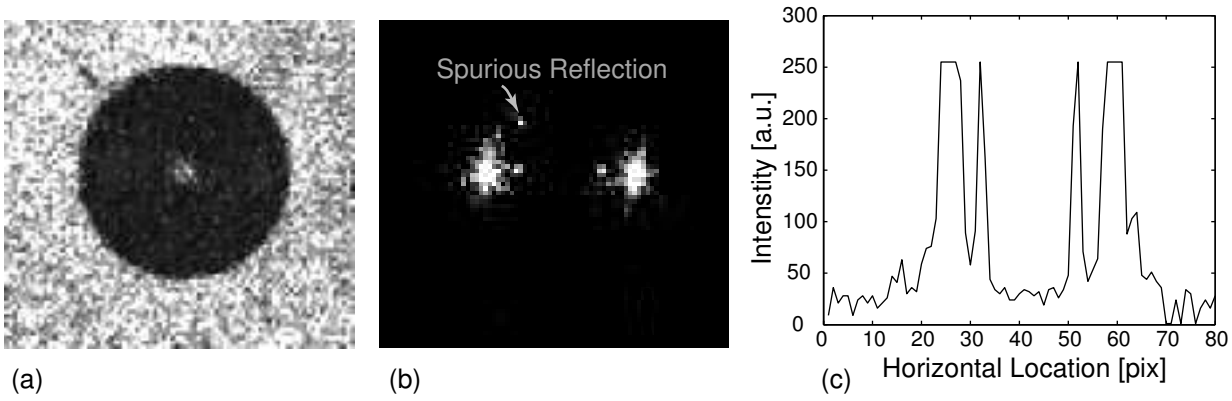

Figure 10: Picture of entrapped bubble at 90° (a) Green channel (b) Red channel (c) Horizontal profile of pixel intensity versus location

4 Discussion

The technique as presented here is already able to give 2D information concerning the size and velocity of the bubbles with a single camera. But, as was mentioned in the introduction, the velocity of the surrounding fluid is also very important in order to model the interaction. Typically this would be done by adding fluorescent tracers to the flow and using a second camera (with appropriate colour filter). However, it is possible to achieve this with only one camera if a colour camera is used. The resulting simple and robust setup that follows, will improve the accuracy of current two phase measurements drastically.

Compared to backlighting the present technique has several important benefits. One advantage is the ability to measure in higher void fractions due to the fact that only the bubbles in the laser-sheet are detected. This localisation of the information also allows us to measure the void fraction, which is a very important quantity in numerical simulations of bubbly flows. The possibility to extract additional information concerning the refractive index or the misalignment is also a positive point. But, maybe the most important benefit of this technique is its suitability to be incorporated in true two phase measurements where, next to information about the bubble, also the velocity of the surrounding fluid is measured.

The comparison with ILIDS will be based on the implementation to bubbly flows as suggested by Niwa et al. [2000]. From a figure similar to Figure 2, the authors concluded that 45° is the best angle to perform ILIDS on bubbles. Since the principle of both techniques is the same, this angle was investigated with our numerical tools as well. In this case externally reflected (N=1) and refracted light (N=2) have the same intensity and both glare points lie very close to one another (the conversion factor equals 8,4). More importantly, ILIDS is more sensitive to a misalignment of the camera. A misalignment of 1° leads to a relative error of 3,3% in the conversion factor at 45°, whereas it is only 1,0% at 96° (and 0,05% for extended GPVS). This is, of course, in favour of the proposed technique. Concerning the error made by the assumption of sphericity, the relative error in α made at an angle of 45° is 15,2%, which lies between basic (16,8%) and extended GPVS (11,4%). Another disadvantage of using ILIDS on bubbly flows as done by Niwa et al. [2000] is that this oblique angle results in a strong horizontal optical compression of the flow limiting the allowable void fractions, which was already quite small due to the strong magnification of the interference pattern. Observing the glare points in focus at an angle of 96° distinctly increases this maximum void fraction. The velocity determination capability of ILIDS is also crippled by this observation angle, since the projection error made in the (horizontal) velocity measurement becomes quite big. Both disadvantages will even be worse in reality since the extra deflection at the wall will result in an actual observation angle of 20° if no extra precautions are taken. But there is also a more fundamental reason why GPVS will be more accurate than ILIDS in measuring velocities. In this case a cross-correlation of two images is used. However, the interference 'discs' are quite large resulting in very flat cross-correlation peaks, which does not allow a very good velocity measurement. Another inherent problem for the velocity determination was mentioned by Damaschke et al. [2002], who compared in-focus and out-of-focus images taken simultaneously. They noticed that a 2D calibration was needed in order to localise the out-of-focus bubbles correctly, partly because the magnification depends on the degree the camera is placed out of focus. This extra calibration will undoubtedly add to the uncertainty of the velocity measurements. In fact, the poor velocity measurements lead several authors (Damaschke et al. [2002], Dantec Dynamics [2003]) to use a second camera that records the bubbles in focus in order to obtain a more accurate velocity measurement. Therefore, it is only logical to assume that GPVS, which records in focus at an angle closer to 90° will have a better accuracy in the

velocity determination. In fact, the velocity determination will most probably be as accurate as PTV measurements if a double frame camera is used. Another major advantage of the new technique is its possibility to give extra information concerning the bubble (refractive index, non-sphericity) and the ability to extract the correct size information, even when spurious reflections are visible. The main advantage of ILIDS at this point is its ability to measure accurately very small particles while maintaining a large field of view. This argument will certainly lose some of its value as the CCD-cameras continue to improve. But again, the most important advantage of GPVS compared to ILIDS is probably the ability to obtain information concerning the bubble size *and* velocity (which are equally accurate), next to the velocity of the surrounding fluid with a low-cost setup.

5 Conclusions

A new bubble measuring technique was presented based on the appearance of glare points. The technique is able to give localised 2D information concerning diameter and velocity of the bubble under an observation angle of 96°. It is also possible to extract information concerning a possible misalignment of the system or the relative refractive index of the bubble. The technique is also able to reject misreadings. The size determination was shown to agree within 1,3% with backlighting. Velocity measurements were performed with streak velocimetry and these results were in line with existing correlations. A measurement of the relative refractive index of a silicone block gave a difference of 1,3% with previous refractive index measurements. In addition, the theoretical dependency of the relative glare point position in function of the observation angle was experimentally verified. The theoretical curve was well within the experimental uncertainty and the maximum error between experiment and theory was 1,5%. Finally, measurements under an observation angle of 90° were performed and the calculated size differed only by 1% with the result from backlighting.

6 Acknowledgements

This research was funded with fellowship SB-031241 granted by the Flemish Institute for the Promotion of Scientific and Technological Research in the Industry (IWT).

References

Y. Akasaka, T. Kawaguchi, and M. Maeda. Application of interferometric laser imaging technique to a transient spray flow. In *11th International Symposium on Applications of Laser to Fluid Mechanics*, Lisbon, 2002.

N. M. Aybers and A. Tapucu. *Waerme-Stoffuebertragung*, 2:171–177, 1969.

R. Clift, J.R. Grace, and M.E. Weber. *Bubbles, drops and particles*. Academic Press, New York, 1978.

N. Damaschke, H. Nobach, T.I. Nonn, N. Semidetnov, and C. Tropea. Size and Velocity Measurements with the Global Phase Doppler Technique. In *11th international symposium on application of laser techniques to fluid mechanics*, Lisbon, 2002.

Dantec Dynamics. Flowmap Particle Sizer. *Dantec Dynamics Newsletter*, 10(7), 2003.

R. L. Datta, D.H. Napier, and D.M. Newitt. *Trans. Inst. Chem. Eng.*, 28:14–26, 1950.

R.M. Davies and Sir G.I. Taylor. *Proc. Roy. Soc., Ser.*, 200:375–390, 1950.

A.R. Glover, S.M. Skippon, and R.D. Boyle. Interferometric laser imaging for droplet sizing: a method for droplet-size measurement in sparse spray systems. *Applied Optics*, 34:8409–8421, 1995.

C.F. Hess. Planar particle image analyzer. In *9th International Symposium on Applications of Laser Techniques to Fluid Mechanics*, Lisbon, 1998.

G. Koenig, K. Anders, and A. Frohn. A new light-scattering technique to measure the diameter of periodically generated moving droplets. *Journal of Aerosol Sciences*, 17:157–167, 1986.

Y. Niwa, Y. Kamiya, T. Kawaguchi, and M. Maeda. Bubble sizing by interferometric laser imaging. In *10th International Symposium on Application of Laser Techniques to Fluid Mechanics*, Lisbon, 2000.

A. Ramuzat. *Techniques de mesures non-invasives appliquees aux ecoulements biologiques: Etude des bifurcations pulmonaire succesives*. PhD thesis, Universite Paris XII, 2002.

R. Theunissen. Improvements in hybrid piv/ptv algorithms and droplet sizing. Master's thesis, Technische Universiteit Delft, 2003.

J.P.A.J. van Beeck, D. Giannoulis, L. Zimmer, and M.L. Riethmuller. Global rainbow thermometry for droplet-temperature measurement. *Optics letters*, 24(23):1696–1698, 1999.

H.C. van de Hulst and R.T. Wang. Glare points. *Applied Optics*, 30(33):4755–4763, 1991.

L. Zimmer. *Etude numerique et experimentale de la turbulence en ecoulement gaz-gouttelettes - Applications aux rideaux d'eau en presence de vent lateral*. PhD thesis, Von Karman Institute for Fluid Dynamics, 2001.